Biomass-derived carbon quantum dot: “On–off-on” fluorescent sensor for rapid detection of multi-metal ions and green photocatalytic CO2 reduction in water

Biomass-derived carbon quantum dot: *"On-off-on"* fluorescent sensor for rapid detection of multi-metal ions and green photocatalytic CO_2 reduction in water

Sebastian Raja[a,b]*, Gelson T.S.T. da Silva[a], Sellamuthu Anbu[c], Caue Ribeiro[a,b] Luiz H. C. Mattoso[a]

[a]*National Nanotechnology Laboratory for Agribusiness (LNNA), Embrapa Instrumentação, São Carlos-SP, 13560-970, Brazil*

[b]*Department of Chemistry, Federal University of São Carlos (UFSCar), 13565-905, São Carlos, São Paulo, Brazil*

[c]*Depts. of Chemistry and Biomedical Sciences, University of Hull, Cottingham Road, Hull, HU6 7RX, UK.*

*Email: sebastianrajaorg@gmail.com. http://orcid.org/0000-0003-4648-5624

ABSTRACT: We have developed carbon quantum dots (CQDs) with excellent photoluminescence (PL) properties from macaúba (*Acrocomia aculeate*) fibers; a widely available cellulosic biomass species of palm trees in South America. As-prepared CQDs showed quasi-spherical morphology with high aqueous solubility and strong excitation-dependent fluorescence behaviour. Interestingly, the CQDs display fluorescence 'turn-off' response with excellent sensitivity toward multi-metal ions including Fe^{3+}, Cu^{2+} and Hg^{2+} with very low detection limits of 0.69 µM, 0.99 µM, 0.25 µM, respectively. Notably, ascorbic acid (AA) induced a change in the (turn-off) fluorescence of

Fe^{3+}-CQDs, which caused an almost 70% revival of fluorescence (turn-on) by displacing Fe^{3+} ions. We have also harnessed CQDs as the visible-light-induced photocatalyst to reduce CO_2 in water. Especially, the CQDs efficiently promote the photocatalytic reduction of CO_2 into methane (CH_4) with an evolution rate of 99.8 nmol/g at 436 nm in aqueous conditions. This indicates that the CQDs provide abundant active sites for CO_2 adsorption and thus enhance the separation and migration of photo-induced charge carriers that efficiently reduce CO_2 into CH_4 without any co-catalyst in 100% water.

Keywords: Macaúba, Carbon quantum dots, Metal ion detection, On-off-on, Visible-light, Photocatalytic CO_2 reduction

1. Introduction

Carbon quantum dots (CQDs) are a novel class of emerging fluorescent nanoparticles (NPs) with discrete and quasi-spherical morphology, consisting mostly of carbon atoms with sizes smaller than 10 nm. Since the discovery of CQDs by Xu *et al*. in 2004 [1], much attention has been paid to the development of these fascinating nanomaterial systems as they are easily be synthesized from two main routes: top-down and bottom-up, including laser ablation, chemical oxidation, arc discharge, solvothermal, hydrothermal, and microwave reactions by using diverse chemical and natural precursors [2, 3]. Notably, CQDs derived from natural precursors are of great interest because of their low-cost, carbon-rich nature, wide availability, facile synthetic approach, and environmentally benign [4-6]. Moreover, converting such low-cost natural precursors into value-added products is a crucial and economical way for waste management since it allows to put up the solid wastes into valuable products [7]. Among all the methods of CQD synthesis, the hydrothermal approach is renowned and the most popular due to its simple, greener, and economic point of view. Recently, biomass residues including banana peels [8], watermelon peel [9], peanut husks [10], Leek [11], waste rice straw [12], Kentucky bluegrass [13], pineapple [14] agro-industrial residues [15-19], have been utilized as a renewable carbon feedstock for the generation of CQDs. Moreover, strong fluorescence properties, chemical inertness, high resistance to photobleaching, tunable photophysical behaviors, and facile surface modification enable CQDs potential nanomaterial candidates for chemosensing [20], photocatalysis [21], energy [22], and biomedical [23, 24] applications.

Ferric ion (Fe^{3+}) plays critical roles in a wide range of biological and environmental processes such as intracellular anion transport, enzymatic reaction, oxygen-carrying, and various bio-syntheses [25, 26]. Some human diseases such as anemia, liver damage, hemochromatosis, and Alzheimer's disease are closely associated with the concentration of Fe(III) ions [26, 27]. Similarly, a comprehensive report on Cupric (Cu^{2+}) ion-based compounds has been utilized in a range of both biological and environmental reactions [28-32]. Also, heavy metal like mercuric (Hg^{2+}) ion is highly toxic even in lower concentration, causing DNA damage to the kidney and neurological disorders [31-33]. Thus, monitoring or regulating such M^{n+} ions in biological and environmental scenarios is vital. Several techniques including electrochemical [34], atomic absorption spectrometry [35], colorimetry [36], and plasma-optical emission spectrometry [37] have been investigated for the detection of M^{n+} ions. In recent years, the development of CQDs-based fluorescent sensors for detecting metal ions is becoming a promising area of chemosensor research due to their simple sampling protocols, high selectivity, and rapid detection. By using this technique, various M^{n+} ions including Fe^{3+} [14, 16, 38-42], Cu^{2+} [17, 29, 43-45], Hg^{2+} [46, 47], Cr^{6+} [48, 49], Al^{3+} [50], and etc. have already been investigated as single analyte-specific systems. But, CQDs with multiple analytes-responsive fluorescent sensors are sparse in the literature [31-33, 51]. Such a platform is essential to detect multiple analytes at a single solution.

Besides, the CQDs-based sensor materials can also be used to develop chip-like optoelectronic devices due to their compact space and economic point of view [31, 32]. For instance, different types of CQDs, including N-doped systems, have been used for the simultaneous detection of a range of metal ions such as Co^{2+}, Fe^{3+}, Cu^{2+}, Pb^{2+}, Hg^{2+}, and Fe^{3+} with the significantly lower limit of detections (LODs) in an aqueous medium [31-33]. Therefore, exploring the novel CQDs as a single fluorescent probe for detecting multiple metal ions will allow them to harness high-performance carbon nanomaterials for environmental applications.

On the other hand, using CQDs as the photocatalysts in CO_2 reduction reactions is a promising approach since they mimic natural photosynthesis and help to deprive the atmosphere's CO_2 level. It has also been considered one of the most sustainable strategies to mitigate global warming and environmental problems due to the elevated CO_2 levels in the atmosphere [52, 53]. Therefore, the multifunctional properties of CQDs, including reliable stability, chemical inertness, optoelectronics, light-harvesting, and photo-induced electron transfer capability, are allowing them to be harnessed as the most potential catalytic candidates in photochemical reactions, including dye degradation [54], H_2

evolution [55], CO_2 reduction [56] and other chemical reactions [57]. But, efficient light absorption, electron transfer, and separation of photogenerated charge carrier properties of CQDs efficiently promote them as potential visible-light responsive photocatalysts [21, 58, 59]. Various biomass residues have been used as the carbon feedstock for the synthesis of CQDs. Yet, utilization of cellulose-based one, in particular, for the synthesis of CQDs are scarce in the literature. Moreover, most of the reported CQDs showed capability of sensing only single analyte in an aqueous system. Besides, only few CQDs showed the catalytic ability of converting CO_2 in to value-added products *via* visible-light photocatlysis. Therefore, the synthesis of CQDs from the cheap and readily available biomass residues, cellulose-based ones, with improved photophysical properties, is to be exploited as a potential fluorescent nanosensor for multi-metal ions, and visible-light photocatalysts for CO_2 reduction in aqueous conditions is an essential objective.

Acrocomia aculeate (macaúba) [60] is a significant and most abundant biomass precursor from native palm species in tropical regions of South America. The lignocellulosic fibers of macaúba have great potential in industries since they possess high cellulose content [61]. Such components are rich in carbon (C), hydrogen (H) and oxygen (O) elements which serve as an essential resource for the formation of CQDs with high content of hydroxyl (OH) and carboxyl (COOH) functionalities on their surface. Such functionalities trigger the increased aqueous solubility and fluorescence property of CQDs. Recently; we developed CQDs from biomass precursors (i.e., Curauá) and investigated their Fe^{3+} ion sensing efficiencies and cellular imaging applications [62].

Herein, we report highly water-soluble and fluorescent CQDs using macaúba as a renewable carbon feedstock through a green hydrothermal synthetic approach. We have utilised as-synthesised CQDs as a fluorescent "nanoprobe" to detect three different metal ions such as Fe^{3+}, Cu^{2+} and Hg^{2+} ions. Also, we found that the completely quenched photoluminescence (PL) of Fe^{3+}-bound CQDs was almost revived upon the addition of biologically relevant reducing agent Vitamin-C (ascorbic acid-AA), thus resulting in on-off-on behaviour. Moreover, CQDs paves the way to utilize sustainable feedstock as a visible-light-induced photocatalyst for CO_2 reduction in an aqueous medium.

2. Experimental Section

2.1. Chemicals

Macaúba fibers were donated by Embrapa Pantanal, Brazil. Metal chloride salts including NaCl, KCl, $CaCl_2$, $BaCl_2$, $MnCl_2.4H_2O$, $FeCl_2$, $FeCl_3$, $CoCl_2.6H_2O$, $NiCl_2.6H_2O$, $CuCl_2.2H_2O$, $AgCl_2$, $ZnCl_2$, $CdCl_2$, $HgCl_2$, $AlCl_3.6H_2O$ and chromate salts such as Cr_2O_3, $K_2Cr_2O_7$ and ascorbic acid (Vitamin-C) were purchased from Sigma Aldrich, Brazil. All the aqueous solutions were prepared by MilliQ water (18.2 MΩ cm at 25 °C). All the analytical grade reagents were used as purchased.

2.2. Synthesis of CQDs

Macaúba fibers (1.00 g) and sodium hydroxide (1 M, 20 mL) was transferred into a 50 mL of Teflon-lined stainless-steel autoclave and heated to 200 °C for 18 h. Then, the autoclave was allowed to attain room temperature, and the reaction mixture was filtered and centrifuged at 10000 rpm for 10 min to remove the unwanted black precipitates. The supernatant was dialysed in MilliQ water through a dialysis membrane (MWCO of 3500) for a week. The water in the dialysis was changed and added fresh water every 24 h. After the dialysis, the solution was freeze-dried to obtain macaúba-derived CQDs as brownish-yellow solid in 28% yield.

2.3. Characterization of C-dots

FT-IR spectrum of CQDs was recorded on a spectrophotometer (Vertex 70, Bruker, Germany) using the attenuated total reflectance (ATR) method. TEM images of the CQDs were recorded on Tecnai TM G2 F20 equipment through a bright field (BF) detector by depositing a droplet of diluted suspension of CQDs on a carbon microgrid (400 mesh; stained with 1.5% uranyl acetate solution) followed drying. The electronic absorption spectrum of the CQDs was acquired by a Double Beam UV-Vis Spectrophotometer (Shimadzu UV 6300PC equipment). Photoluminescence (PL) emission spectral studies were performed using an RF-5301PC Fluorimeter (Shimadzu, Japan). XPS analysis was done in an Ultra AxisTM spectrometer (Kratos Analytical, Manchester, UK). The samples were irradiated with mono-energetic Al Kα1, 2 radiation (1486.6 eV) and the spectra were recorded data power of 144 W (12 kV x 12 mA). The CQDs was analysed by an FEI Tecnai G2 F20 X-TWIN (200 kV) transmission electron microscope (TEM) (Philips-FEI, Netherlands) with a Gatan CCD camera. The samples were prepared dispersing the material into isopropanol *via* ultrasonication, following dropping in the copper TEM grids coated with formvar-carbon film (Maxtaform, 200 mesh, Plano, Wetzlar, Germany). AFM was measured at Nanosurf (Model: Flex; technique: tapping). Samples were loaded on the surface of mica and dried in the desiccator before analysis.

2.4. Metal (M^{n+}) ion sensing analysis

The CQDs (25 mg) was dissolved in 500 mL of MilliQ water to attain the final concentration of 50 µg/mL of stock solution. The chromates (Cr^{3+}& Cr^{6+}) and chloride salts of metal ions (Na^{+}, K^{+}, Ca^{2+}, Ba^{2+}, Mn^{2+}, Fe^{2+}, Fe^{3+}, Co^{2+}, Ni^{2+}, Cu^{2+}, Zn^{2+}, Ag^{+}, Cd^{2+}, Hg^{2+} and Al^{3+}) were dissolved separately in MilliQ water (1 mM). The aqueous solution of AA was also prepared in deionised water (1 mM). In titration experiments, a 3 mL stock solution of CQDs (50 µg/mL) was taken in a quartz cuvette of 1 cm optical path length. Then, 5-300 µM of each metal ion (1 mM) was added to the stock solution with a micro-pipette. For the fluorescence experiment, the emission maximum (λ_{em}) of CQDs with and without the presence of metal ions was observed between 400 and 700 nm (λ_{ex} = 340 nm) at 298 K. In fluorescence experiments, both excitation and emission slit widths were 3 nm. Each titration was repeated at least twice to get a consistent value. Analysis of the fluorescence intensity (F_0/F) of CQDs as a function of increasing metal ion (Fe^{3+}, Cu^{2+} and Hg^{2+}) concentration ($[M^{n+}]$) was well described by the Stern−Volmer ($F_0/F = 1 + K_{SV}[A]$) equations. K_{SV} value was determined from the slope of the linear plot of (F_0/F vs $[M^{n+}]$).

2.5. pH analysis

The pH-dependent PL emission of CQDs was also carried out. The PL spectra of aqueous CQD solutions (50 µg/mL) at various pH ranges (between 2-12) were acquired using an RF-5301PC Fluorimeter (Shimadzu, Japan) upon excitation at 340 nm at room temperature.

2.6. Photostability

The UV-visible absorption and PL emission intensity of CQD solutions with various irradiation times under UV light (Deuterium (D2) lamp; L6380) was tested. In a typical procedure, 10 mL aqueous solution of CQDs (0. 5 mg) or Rhodamine B (RhB) (0. 4 mg) solution was irradiated in a closed hood at a regular interval for 1 h. Then, the corresponding absorption and emission intensities were recorded on the UV-visible spectrophotometer (Shimadzu UV 6300PC equipment) and fluorescence spectrometer (RF-5301PC Fluorimeter (Shimadzu, Japan).

2.7. Photocatalytic test

The photoreduction reaction of CO_2 was performed in a 250 mL quartz tube equipped with a Teflon stopper. Under continuous magnetic stirring, the experiments were performed at 25 °C in a photoreactor equipped with six

fluorescent lamps (Phillips, 15 W, the maximum intensity at 440 nm) (Fig. S5). In a typical photocatalytic reaction, CQDs (50 mg) was dissolved in distilled water (100 mL) followed by bubbling with high-purity CO_2 gas for 20 min (10 mL min^{-1}) to saturate the reactor to eliminate oxygen completely. After 6 h, the gas phase (1 mL) was collected with a syringe and injected into gas chromatography (TRACE 1300, Thermo Fisher Scientific) equipped with TCD FID detector and 13X Molecular sieve and Porapak N columns. The experiments were also conducted with and without the presence of catalyst and light. The calibration curve method was used to quantify the generated products from CO_2 and compared with an external standard mixed gas. The apparent quantum yield (AQY) of CH_4 was calculated using the actinometric method [63].

3. Results and Discussion

3.1. Synthesis and characterisation

We have used a simple and one-pot synthetic strategy to obtain fluorescent CQDs from *Acrocomia aculeate* fibers, as illustrated in Fig. 1A. Briefly, the hydrothermal carbonization of macaúba fibers with sodium hydroxide (1 M) at 200 °C for 18 h afforded CQDs. After filtration, dialysis, and freeze-drying process, the CQDs were isolated as a brownish-yellow solid. As reported in the literature [62, 64], during the above-mentioned hydrothermal reaction, the cellulose, hemicellulose, and lignin contents of macaúba fiber undergo hydrolysis and yield saccharides and aromatic alcohols. Further, these small molecules are converted into CQDs by dehydration and condensation reactions.

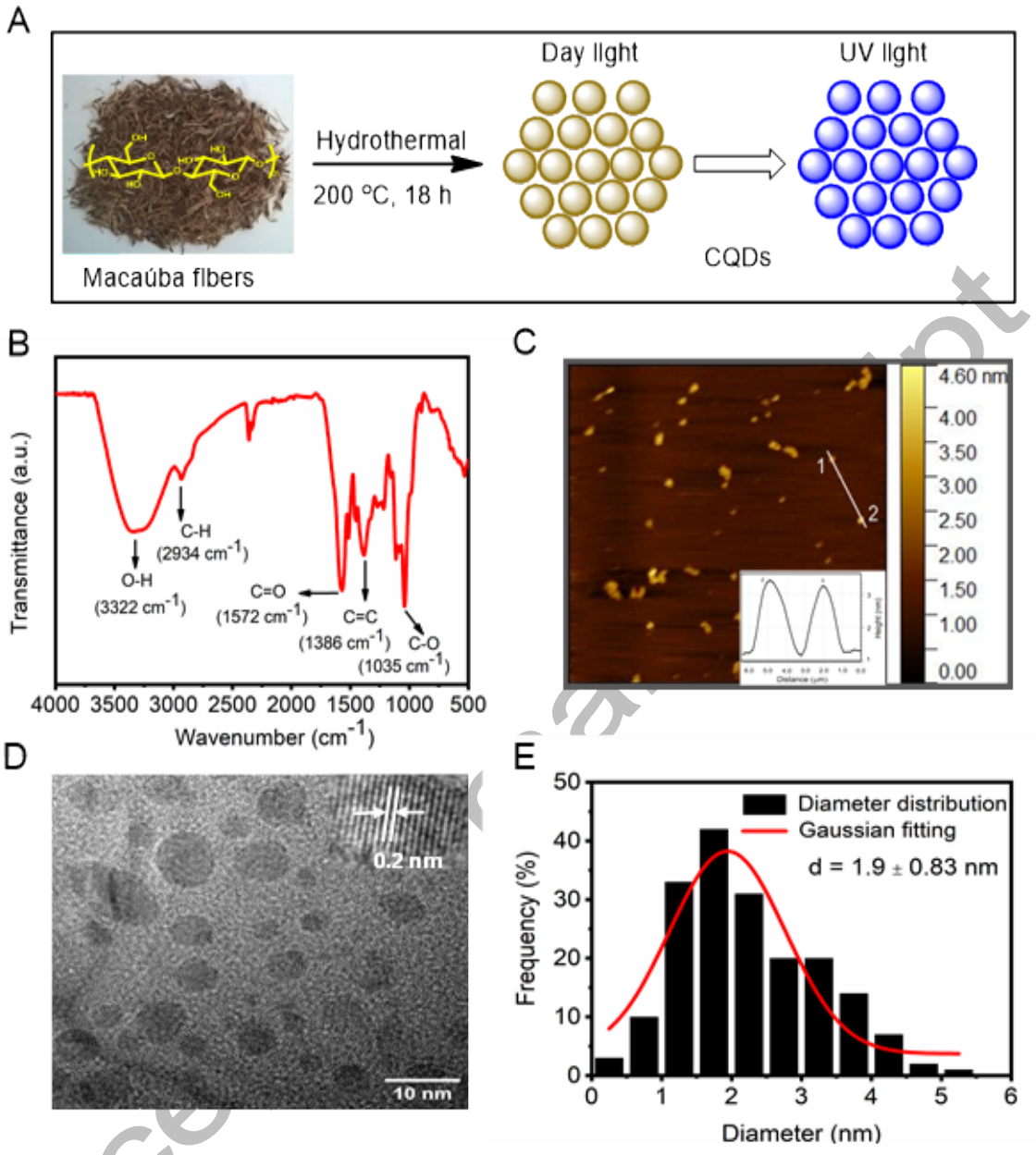

Fig. 1. Synthesis and characterizations of macaúba-derived CQDs. (A) Schematic illustration for the synthesis of CQDs from macaúba fibers. B) Representative ATR-FTIR spectra of CQDs. (C) AFM of CQDs. Inset shows the height profile of CQDs. (D) HR-TEM image of CQDs. Inset shows the lattice fringes of the CQD. (E) Size distribution of CQDs (n > 100) calculated from TEM micrographs.

As shown in Fig.1B, the characteristic FT-IR absorption peaks for O-H and C-H stretching vibrations were observed at 3321 cm^{-1} and 2928 cm^{-1}, respectively. The overlapped peak at 1580 was assigned to C=O and C=C stretching vibrations in the conjugated structure of CQDs. The intensive bands at 1396 cm^{-1} and 1042 cm^{-1} correspond to C-O and =C-H stretching vibrations. Fig.1C illustrates the CQDs' topographic morphology and height distribution, respectively. The height profile of CQDs was found to be approximately 3 nm (Inset). Also, a precise spherical shape with the uniformly dispersed topology of the TEM image confirms the absence of any apparent aggregation (Fig. 1D). The particle size distribution of the CQDs showed a relatively narrow size distribution ranging from 0 to 5 nm with an average diameter of 1.9 nm (n >100) (Fig. 1E). In the XPS survey spectrum as-synthesized CQDs exhibited two peaks at 284.0 and 530.6 eV, which are attributed to the presence of carbon (C) and oxygen (O) atoms, respectively (Fig. 2A). The high-resolution spectrum of the O1s (Fig. 2B) proved the two appropriate oxygen states of C=O (529.1 eV) and C-O (530.4 eV). Moreover, the high-resolution spectrum of the C1s (Fig. 2C) exhibited three prominent peaks at 281.8, 283.4, and 285.8 eV, which were attributed to C-C, C-O, and C=O, respectively. The binding energy peak at 281.8 eV confirmed the graphitic structure (sp^2, C-C) of the macaúba-derived CQDs, consistent with the O1s spectrum. These results revealed that the molecular system of macaúba-derived CQDs mainly consists of abundant carbonyl, carboxylate, and hydroxyl groups [62, 64]. In the XRD pattern, the CQDs own a single broad peak at 22° (2θ) due to the characteristic amorphous carbon phase (Fig.2D), which indicates that the synthesized CQDs are a relatively poor crystalline nature.

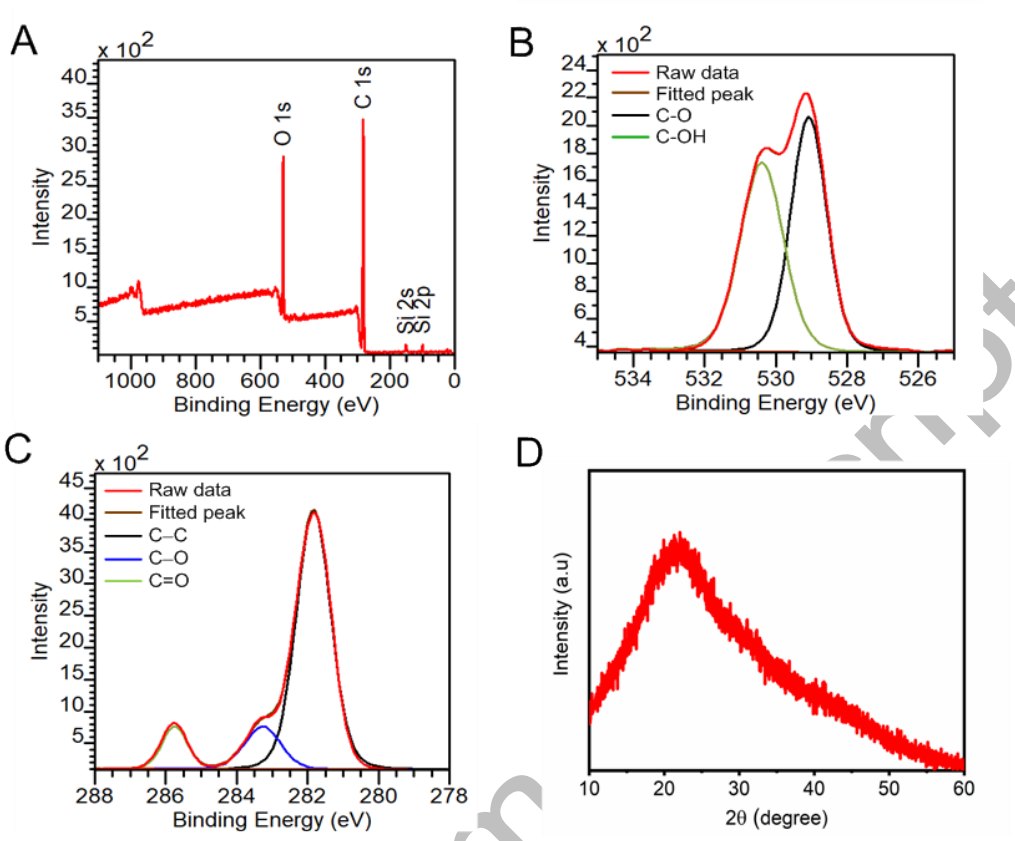

Fig. 2. (A) XPS survey spectrum of CQDs. (B) XPS high-resolution spectrum of O 1s spectrum. (C) XPS high-resolution spectrum of C 1s. (D) XRD spectra of CQDs.

3.2. Photophysical properties

The absorption spectrum (Fig. 3A) of as-prepared CQDs showed a distinct peak at 277 nm that can be attributed to π-π* transition of C=C bonds for carbons consistent with most of the CQDs reported in the literature [14, 16, 42, 62]. A strong emission band at 452 nm was observed upon exciting at 340 nm (Fig. 3A). Further, the CQDs exhibited excitation-dependent PL behavior because their emission shifted from blue to red against the excitation wavelengths ranging from 280 nm to 520 nm (Fig. 3B and S2A). Such PL behavior could be attributed to different-sized particles and the distribution of various surface emissive traps of the CQDs [20].

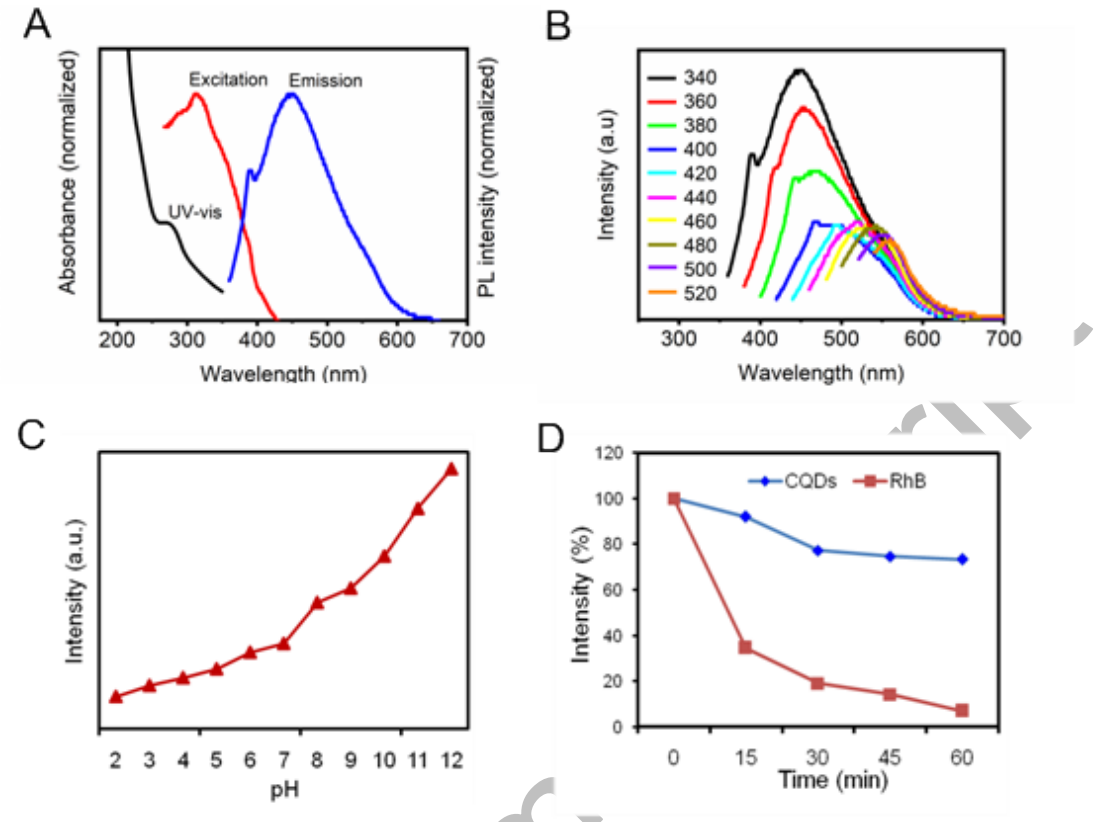

Fig. 3. Physicochemical characterizations of CQDs. (A) UV-visible absorption, excitation, and emission profile of CQDs in aqueous condition at 50 µg mL^{-1} concentration. (B) PL emission spectra of CQDs at different excitation wavelengths ranging from 340 nm to 520 nm with increments of 20 nm. (C) PL emission profile of CQDs under acidic to basic pH ranges. (D) Photostability of CQDs at constant illumination of UV light under various time points

In pH measurements, the PL intensity of CQDs at 452 nm was increased with increasing the pH, which indicates that the CQDs are accessible at a range of pH (6-12) conditions (Fig. 3C). We have also evaluated CQDs' photostability at continuous irradiation using a Deuterium (D_2) lamp for durations of up to 60 min in UV-visible absorption spectroscopy. No apparent changes were observed in the absorbance of CQDs, while the absorbance of the commercial Rhodamine B (RhB) was decreased to □30% (Fig. S1A and B). Under similar experimental conditions, PL intensity of RhB lost almost 100% in 60 minutes, whereas CQDs lost only 20% at continuous illumination of UV light (Fig. 3D). It reveals that CQDs showed superior photostability than commercial RhB dye,

consistent with earlier findings [62, 65]. We also analysed the surface charge of the CQDs from acidic to basic pH ranges resulting high negative zeta potential at neutral PH (Fig. S2B). Further, the ionic stability of CQDs was examined at different concentrations of NaCl ranging from 0 to 1 M (Fig. S3). No apparent changes in the PL intensity of CQDs at 450 nm were observed even at a higher concentration of NaCl (1 M), suggesting that CQDs owe excellent ionic strength even at higher concentrations.

3.3. Multi-metal (M^{n+}) ion detection

The metal ion (M^{n+}) sensing capability of CQDs was studied by the PL emission spectroscopic method. In aqueous conditions, the CQDs show a strong PL emission peak *ca.* at 452 nm upon excitation at 340 nm. As shown in Fig. 4A and 4B, only Fe^{3+}, Cu^{2+}, and Hg^{2+} ions elicited significant PL emission quenching response over a range of other metal ions (M^{n+}), which exhibit almost no effective quenching responses under identical conditions. In the competitive analysis, Fe^{3+} ion showed higher sensing performance than other M^{n+} ions as a result of strong fluorescence quenching (Fig. 4B). This is mainly due to the strong affinity between many hydroxyl and carboxyl functionalities on the surface of CQDs and M^{n+} ions that facilitate an enhanced charge-transfer mechanism [31, 32]. The strong PL quenching of CQDs with Fe^{3+}, Cu^{2+} and Hg^{2+} could be attributed to the transfer of an electron from the excited state of CQDs to the vacant 3d orbital of the above-mentioned M^{n+} ions, resulting in nonradiative electron-hole recombination [42].

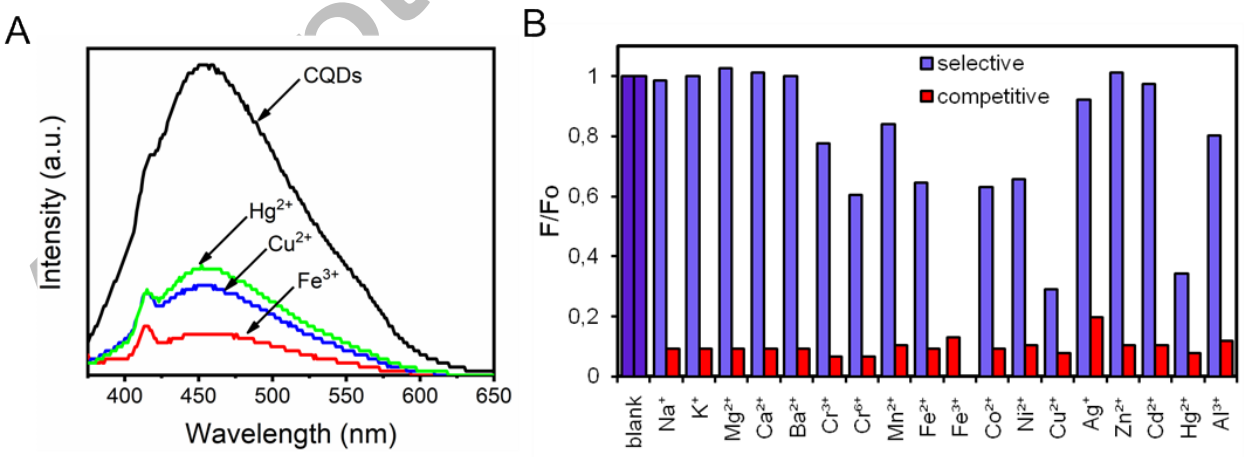

Fig. 4 PL intensity profiles of CQDs at the excitation wavelength of 340 nm (50 μgmL^{-1}) under aqueous conditions. (A) PL intensity of CQDs against Fe^{3+}, Cu^{2+} and Hg^{2+} ions (0.1 mM). (B) PL intensity of CQDs against various metal (M^{n+}) ions under selective and competitive analysis.

To ascertain the precise metal (Fe^{3+}, Cu^{2+} and Hg^{2+}) ion binding propensity of CQDs, we have carried out fluorescence titration experiments. Upon gradual addition of aqueous Fe^{3+} (0–150 μM), Cu^{2+} (0–195 μM) and Hg^{2+} (0–290 μM) ions to the solution of CQDs, the PL intensity at 452 nm was gradually decreased (Fig. 5A, B and C). Notably, the CQDs show significantly higher PL quenching response (~94%) towards Fe^{3+} (Fig. 5A) over the Cu^{2+} and Hg^{2+} ions, which showed only ~80% and ~71%, respectively (Fig. 5C and E). The linear ranges were observed at 0–30 μM, 0–25μM and 0–60 μM for Fe^{3+} ($R^2 = 0.997$), Cu^{2+} ($R^2 = 0.997$) and Hg^{2+} ($R^2 = 0.998$), respectively (Fig. 5B, D and F). Linear regression equations for Fe^{3+}, Cu^{2+} and Hg^{2+} were found to be $y = 0.204x + 0.769$, $y = 0.095x + 0.909$, $y = 0.080x + 0.902$, respectively. Moreover, the extent of the metal ion sensing capability of the CQDs was determined by the limit of detection (LOD) plots using the literature [42] reported equation: 3δ/m, where δ and m represents the standard deviation and slope of the linear fit, respectively. Quantification of the Fe^{3+}, Cu^{2+} and Hg^{2+} detection of the CQDs by PL titration analysis displays a detection limit (LOD) at a shallow concentration of 0.69×10^{-6}, 0.99×10^{-6} and 0.25×10^{-6} M, respectively, which is more effective than the several reported systems derived from the biomass feedstock (Table 1, 2 and 3), with the additional advantage of multi-metal ion detection. All these observations indicate that the macaúba-derived CQDs is the promising sensor candidate in detecting trace amounts of the above-mentioned M^{n+} ions in the environmental and biological scenarios.

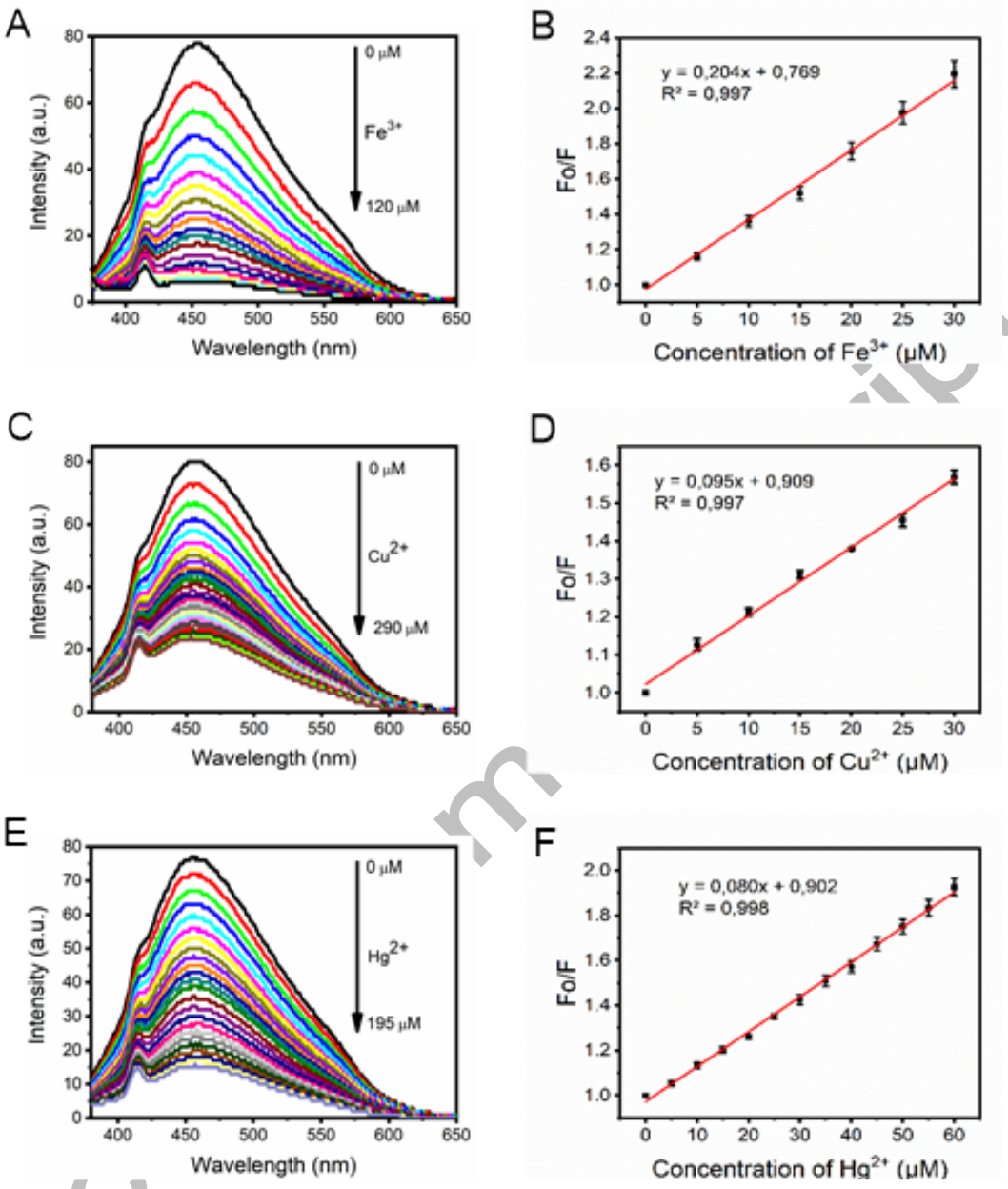

Fig. 5. PL emission titration profiles of CQDs (50 μg mL^{-1}) with different metal (Fe^{3+} (0-100 μM), Cu^{2+} (0-290 μM), and Hg^{2+} (0-195 μM) ions in water (A, C and E): (B) (D) and (F) Linear relationship of the change in the PL intensity at 452 nm versus the concentration of Fe^{3+}, Cu^{2+} and Hg^{2+}, respectively. Error bar indicates mean ± standard deviation.

Table 1. Detection of Fe^{3+} ions by representative CQDs derived from various natural sources.

Carbon source	**Passivating agent**	**Linear range (μM)**	**LOD (μM)**	**Reference**
Cellulose	Ammonia	0-100	1.14	19
Lignin	-	0-300	0.77	40
Actinidia Deliciosa	Ammonia	5-25	0.85	42
Ananas erectifolius	-	0-30	0.77	62
Crop biomasses	-	0-500	5.23	64
Dwarf banana peel	-	5-25	0.66	66
Cranberry beans	-	30-600	9.55	67
Acrocomia aculeate	-	0-30	0.69	This work

Table 2. Detection of Cu^{2+} ions by representative CQDs derived from various natural sources.

Carbon source	**Passivating agent**	**Linear range (μM)**	**LOD (μM)**	**Reference**
Acacia Concinna	-	0.01- 10	0.0043	68
Lily Bulbs	-	0.05–2.0	0.0012	69
Spirulina powder	-	0.01–0.1	0.011	70
Coccinia Indica	L-cysteine	0-0.025	0.045	71
CitricAcid	PEI	0.37–2.5	0.63	72

Acrocomia Aculeate	-	0-25	0.99	This work

Table 3. Detection of Hg^{2+} ions by representative CQDs derived from various natural sources.

Carbon source	**Passivating agent**	**Linear range (μM)**	**LOD (μM)**	**Reference**
Psidium Guajava	-	6-38	82	73
Citric Acid	melamine	2-14	0.44	74
Hongcaitai	-	0.2 - 15	0.06	75
Cellulose	Ionic liquid	6–80	1.6	76
Citric Acid	diethylenetriamine	0–80	0.20	77
Highland Barley	ethanediamine	10–160	0.48	78
Acrocomia Aculeate	-	0-60	0.25	This work

3.4. "On-off-on" response of CQDs

To confirm whether the Fe^{3+} detection event (on-off) of CQDs is reversible, an equivalent of ascorbic acid (AA) solution was added into the aqueous solution of CQDs, which was preincubated with an equivalent of Fe^{3+} solution (Fig. 6A, B and C). Interestingly, AA influences the Fe^{3+} quenched CQDs as consequences of the revival of the PL intensity was found to be nearly 70% (Fig. 6D). This phenomenon could be due to the redox reaction between the CQDs-Fe^{3+} and AA, in which Fe^{3+} can be reduced to Fe^{2+} by AA (Fig. 6A) that minimises nonradiative electron transfer and maximises the revival of PL intensity CQDs [45, 79-81]. Gradual increases in the PL intensity of CQDs-Fe^{3+} at 452 nm were observed with increasing the concentration of AA (0–150 μM) (Fig. S4A). The linear relationship of the PL intensity of CQDs-Fe^{3+} concerning the concentration of AA was observed in the range of 5–50 μM (Fig. S4B) with 4.6×10^{-6}M of LOD. No apparent changes were observed for CQDs-Fe^{3+} against Cu^{2+} and Hg^{2+}

ions while treating with AA (data not shown). It indicates that the macaúba-derived CQDs can be developed as a potential probe in the nanosensor platform for the rapid detection of AA.

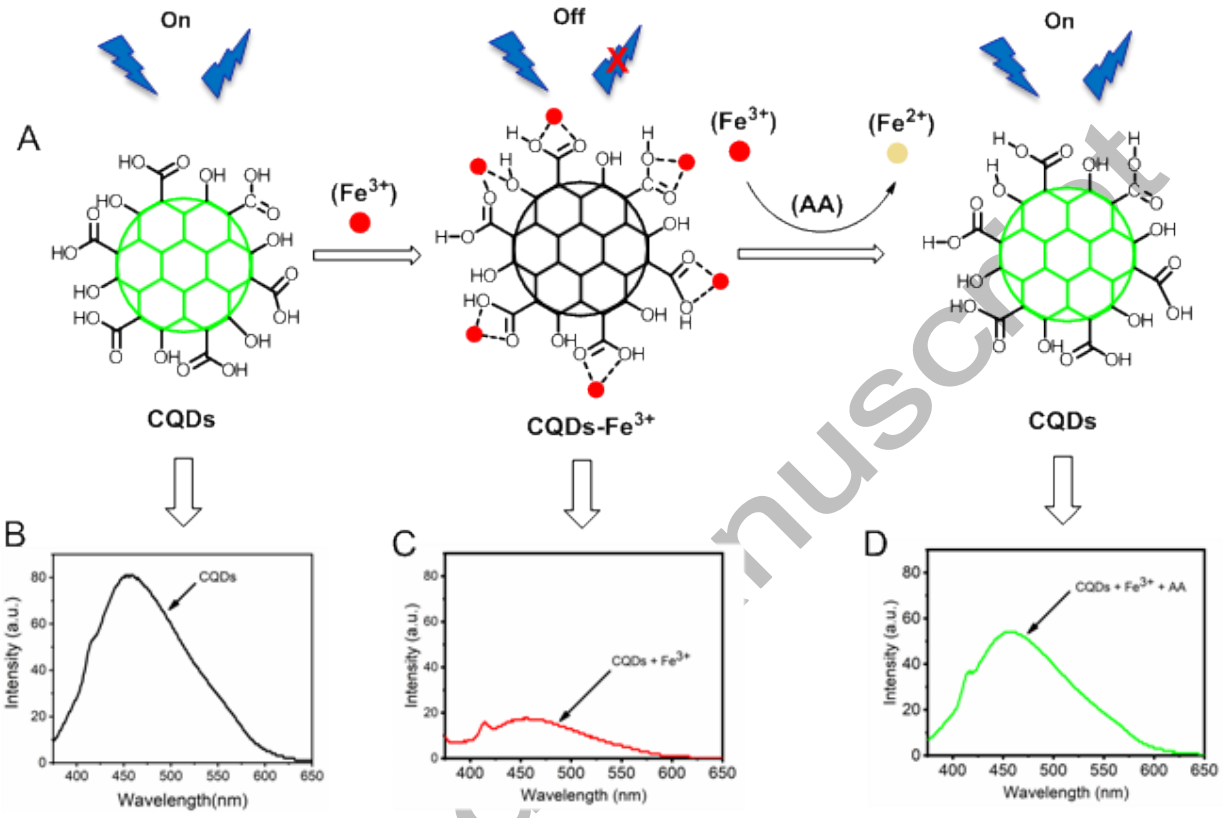

Fig. 6. Fluorescence "on-off-on" profiles of CQDs (50 μg mL^{-1}). (A) Illustration of CQDs interaction with Fe^{3+} and AA in an aqueous medium. (B, C and D) Representative PL intensity profile of CQDs

3.5. Photocatalytic CO_2 reduction

To test the photocatalytic activity of CQDs, we have used them as a potential catalyst in a CO_2 reduction reaction. For that, the CQDs (50 mg) in MilliQ water (100 mL) were taken in a quartz tube equipped with a Teflon stopper and saturated the reaction mixture with high purity CO_2 gas, and kept under visible-light for 6 h at 25 °C. After 6 h, we observed the formation of CH_4 and found no traces of typical gases including CO_2, CO and H_2 in the quartz reaction chamber. However, in the absence of CQDs, the standard gases include CO_2, CO and H_2 being encountered.

This indicates that the CQDs serve as an active photocatalyst that promotes the complete and selective reduction of CO_2 into CH_4 in the presence of visible-light. Also, the significant conversion of CH_4 (99.8 nmol/g) from CO_2 (Fig. 7B) confirms that the CQDs material could be considered as the suitable candidate for photocatalytic reaction. This behaviour could be due to the photoreduction of hydroxyl groups at the surface of the CQDs as a plausible photoreduction mechanism of CO_2 shown in Fig. 7A [82]. This mechanism includes the physisorption of the CO_2 on photocatalytic CQDs surface due to the presence of a large number of hydroxyl functionality and activation of CQDs by visible light irradiation, which generates charge carriers inducing reductive and oxidative processes. In the highest occupied molecular orbital level (HOMO), the water is oxidised to produce H^+ and molecular oxygen while the excited electron transfers from the lowest unoccupied molecular orbital (LUMO) to the CO_2 molecules, generating CO_2 species [82-86]. Recently, CQDs as a bare photocatalyst showed outstanding performance for reducing CO_2 to methanol with 100% yield under solar-driven photocatalytic reaction in water [60]. Similarly, CQDs decorated carbon nitride (g-C_3N_4) showed excellent catalytic performance of CO_2 photoreduction to yield CH_4 (25%) under UV light [59]. Our findings from this investigation pave the way to utilize macaúba-derived CQDs as an efficient visible-light-induced photocatalyst to reduce CO_2 into CH_4 without doping any co-catalyst.

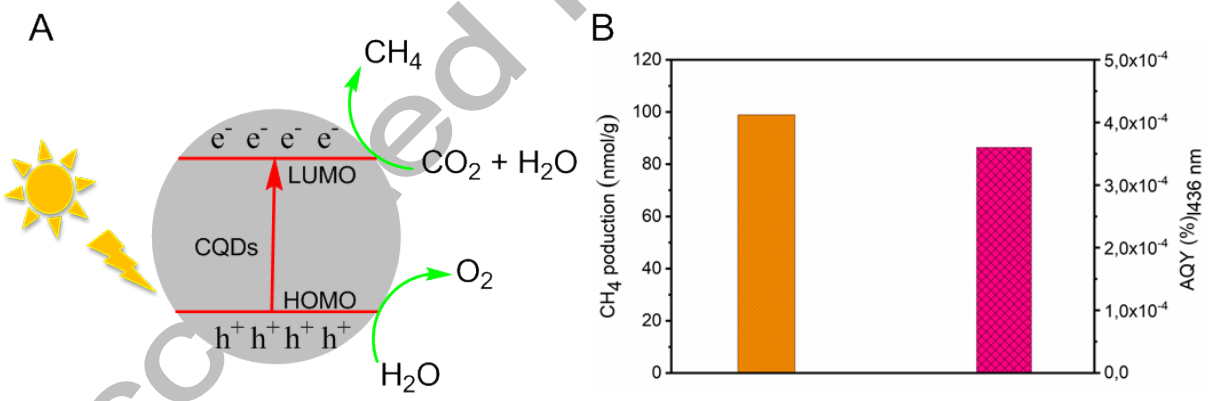

Fig. 7. Photocatalytic reduction of CO_2 into CH_4 in an aqueous medium. A) Plausible mechanism of CQDs. B) Selective production of CH_4. System: CQDs in H_2O; Concentration of the catalyst: 500 mg L^{-1}. Samples were filled with CO_2 and illuminated by a fluorescence lamp.

4. Conclusions

In summary, a facile one-pot hydrothermal approach for synthesising highly fluorescent CQDs from cellulosic biomass waste (macaúba fibres) as the green carbon feedstock has been demonstrated. The obtained quasi-spherical CQDs with a graphitic structure own an average diameter of 1.9 nm and –COOH, –OH surface functional groups that provide high water solubility. Without any surface passivation, as-synthesized CQDs showed excellent performance as multianalyte fluorescent sensor systems for detecting Fe^{3+}, Cu^{2+} and Hg^{2+} ions with very low detection limit of 0.69 μM, 0.99 μM, and 0.23 μM, respectively, in an aqueous medium. Notably, CQDs demonstrate favorable "on-off-on" behaviour as a function of selective recovery of fluorescence quenched by Fe^{3+} ions using ascorbic acid (AA). Besides, CQDs with promising physicochemical properties could reduce CO_2 into CH_4 under visible-light irradiation without any co-catalyst. Altogether, facile synthesis, excellent photophysical properties and multiple surface functionalities enable macaúba-derived CQDs as a potential nanomaterial candidate in sensing and photocatalysis. This work paves the way to exploit biomass waste into value-added products in favor of environmental protection.

Ethics approval and consent to participate This work does not involve human subjects.

Consent for publication All authors consent to publish this work.

Availability of data and materials All data generated or analysed during this study are included in this article (and its supplementary information files).

Competing interests The authors have no competing interests to reveal.

Funding This work was financially supported by Brazilian federal government agency (CAPES) - Proc. No. 88887.575987/2020-00 and the São Paulo Research Foundation (FAPESP) - Proc. No. 2015/00094-0 and Proc. No. 2017/22017-3.

Authors' contributions: Sebastian Raja: Conceptualization, Methodology, Writing- Original draft preparation, Investigation and visualization. **Gelson T.S.T. da Silva:** Investigation. **Sellamuthu Anbu:** Validation. **Caue Ribeiro:** Supervision. **Luiz H. C. Mattoso:** Supervision

.

Authors' information Sebastian Raja: Young Talent Researcher, Embrapa Instrumentação. Gelson T.S.T. da Silva: Postdoctoral Researcher, Embrapa Instrumentação. Sellamuthu Anbu: Postdoctoral Researcher, University of Hull. Caue Ribeiro: Researcher, Embrapa Instrumentação. Luiz H. C. Mattoso: Senior Researcher, Embrapa Instrumentação.

Acknowledgements The authors thank CAPES (Proc. No. 88887.575987/2020-00) and FAPESP (Proc. No. 2015/00094-0; Proc. No. 2017/22017-3) for financial support. S. Anbu gratefully acknowledges the Depts. of Chemistry and Biomedical Sciences, University of Hull, UK and RSC for the award of Research Fund grant (RF19-7464). The authors thank FAPESP (Proc. No. 2018/01258-5) for financial support. The authors also thank the Center for the Development of Functional Materials – CDMF / Sao Paulo Research Foundation – FAPESP (Proc. No. 2013/07296-2).

References

1. Xu X, Ray R, Gu Y, Ploehn HJ, Gearheart L, Raker K, Scrivens WA (2004) Electrophoretic Analysis and Purification of Fluorescent Single-Walled Carbon Nanotube Fragments. J Am Chem Soc 126:12736-12737. https://doi.org/10.1021/ja040082h.

2. Đorđević L, Arcudi F, Cacioppo M, Prato M (2022) A multifunctional chemical toolbox to engineer carbon dots for biomedical and energy applications. Nat Nanotechnol 17:112-130. https://doi.org/10.1038/s41565-021-01051-7.

3. Zhang L, Yang X, Yin Z, Sun L (2022) A review on carbon quantum dots: Synthesis, photoluminescence mechanisms and applications. Luminescence 37:1612-1638. https://doi.org/10.1002/bio.4351.

4. Huang J, Liu J, Wang J (2020) Optical properties of biomass-derived nanomaterials for sensing, catalytic, biomedical and environmental applications. Trac-trends Anal Chem 124:115800. https://doi.org/10.1016/j.trac.2019.115800.

5. Wareing TC, Gentile P, Phan AN (2021) Biomass-Based Carbon Dots: Current Development and Future Perspectives. ACS Nano 15:15471-15501. https://doi.org/10.1021/acsnano.1c03886.

6. Raja S, Mattoso LHC, Moreira FKV (2019) Biomass-derived nanomaterials, in: Rajendran S, Naushad M, Balakumar S (Eds) Nanostructured Materials for Energy Related Applications. Environmental Chemistry for a Sustainable World 24 Springer Cham pp 243-270. https://doi.org/10.1007/978-3-030-04500-5_10.

7. Raja S, Hamouda AEI, Toledo MAS, Hu C, Bernardo MP, Schalla C, Leite LSF, Buhl EM, Dreschers S, Pich A, Zenke M, Mattoso LHC, Sechi A (2021) Functionalized Cellulose Nanocrystals for Cellular Labeling and Bioimaging. Biomacromolecules 22:454-466. https://doi.org/10.1021/acs.biomac.0c01317.

8. Nguyen TN, Le PA, Phung VBT (2022) Facile green synthesis of carbon quantum dots and biomass-derived activated carbon from banana peels: synthesis and investigation. Biomass Conv Bioref 12:2407-2416. https://doi.org/10.1007/s13399-020-00839-2.

9. Han L, Zhu P, Liu H, Sun B (2022) Molecularly imprinted bulk and solgel optosensing based on biomass carbon dots derived from watermelon peel for detection of ethyl carbamate in alcoholic beverages. Microchim Acta 189:286. https://doi.org/10.1007/s00604-022-05388-1.

10. Sivakumar K, Suvitha S, kanna SKR, Ponnusamy M (2022) Development of peanut husk carbon quantum dots and ferrite foil epoxy composite for EMI shielding at high frequency bands. Biomass Conv Bioref. https://doi.org/10.1007/s13399-022-03469-y.

11. Wu L, Long R, Li, T. Tang C, Tong X, Guo Y, Shi S, Xiang H, Tong C (2020) One-pot fabrication of dual-emission and single-emission biomass carbon dots for Cu^{2+} and tetracycline sensing and multicolor cellular imaging. Anal Bioanal Chem 412:7481-7489. https://doi.org/10.1007/s00216-020-02882-4.

12. Kumari M, Chaudhary GR, Chaudhary S, Huang M, Guo Z (2022) Transformation of waste rice straw to carbon quantum dots and their potential chemical sensing application: green and sustainable approach to overcome stubble burning issues. Biomass Conv. Bioref. https://doi.org/10.1007/s13399-022-02761-1.

13. Krishnaiah P, Atchudan R, Perumal S, Salama E, Lee YR (2022) Utilization of waste biomass of Poa pratensis for green synthesis of n-doped carbon dots and its application in detection of Mn^{2+} and Fe^{3+}. Chemosphere 286:131764. https://doi.org/10.1016/j.chemosphere.2021.131764.

14. Gupta DA, Desai ML, Malek NI, Kailasa SK (2020) Fluorescence detection of Fe^{3+} ion using ultra-small fluorescent carbon dots derived from pineapple (Ananas comosus): Development of miniaturized analytical method. J Mol Struct 1216: 128343. https://doi.org/10.1016/j.molstruc.2020.128343.

15. Brachi P (2022) Synthesis of fluorescent carbon quantum dots (CQDs) through the mild thermal treatment of agro-industrial residues assisted by γ-alumina. Biomass Conv Bioref 10: 1301–1312. https://doi.org/10.1007/s13399-019-00503-4.

16. Li S, Chen X, Cheng Z, Luo S, Nguyen TT, Guo M, Gao X (2021). Promoting effect of cellulose-based carbon dots at different concentrations on multifunctional photocatalytic degradation of dyes by ZnO. Opt Mater 121:111591. https://doi.org/10.1016/j.optmat.2021.111591.

17. Zattar APP, Mesquita JP, Pereira FV (2022) Luminescent carbon dots obtained from cellulose and their applications as sensors for metal ions. Mater Chem Phys 290:126633. https://doi.org/10.1016/j.matchemphys.2022.126633.

18. Cheng C, Xing M, Wu Q (2019) A universal facile synthesis of nitrogen and sulfur co-doped carbon dots from cellulose-based biowaste for fluorescent detection of Fe^{3+} ions and intracellular bioimaging. Mater Sci Eng C 99:611–619. https://doi.org/10.1016/j.msec.2019.02.003.

19. Liu Z, Chen M, Guo Y, Zhou J, Shi Q, Sun R (2020) Oxidized nanocellulose facilitates preparing photoluminescent nitrogen-doped fluorescent carbon dots for Fe^{3+} ions detection and bioimaging. Chem Eng J 384:123260. https://doi.org/10.1016/j.cej.2019.123260.

20. Liu ML, Chen BB, Li CM, Huang CZ (2019) Carbon dots: synthesis, formation mechanism, fluorescence origin and sensing applications. Green Chem 21:449-471. https://doi.org/10.1039/C8GC02736F.

21. Saini D, Garg AK, Dalal C, Raj Anand S, Sonkar SK, Sonker AK, Westman G (2022) Visible-Light-Promoted Photocatalytic Applications of Carbon Dots: A Review. ACS Appl Nano Mater 5:3087-3109. https://doi.org/10.1021/acsanm.1c04142.

22. Rasal AS, Yadav S, Yadav A, Kashale AA, Manjunatha ST, Altaee A, Chang J (2021) Carbon Quantum Dots for Energy Applications: A Review. ACS Appl Nano Mater 4:6515-6541. https://doi.org/10.1021/acsanm.1c01372.

23. Alaghmandfard A, Sedighi O, Rezaei NT, Abedini AB, Khachatourian AM, Toprak MS, Seifalian A (2021) Recent advances in the modification of carbon-based quantum dots for biomedical applications. Mater Sci Eng C 120:111756. https://doi.org/10.1016/j.msec.2020.111756.

24. Kailasa SK, Koduru JR (2022) Perspectives of magnetic nature carbon dots in analytical chemistry: From separation to detection and bioimaging. Trends Environ 33: e00153. https://doi.org/10.1016/j.teac.2021.e00153.

25. Rouault T (2014) Iron-Sulfur Clusters in Chemistry and Biology. De Gruyter GmbH & Co KG. https://doi.org/10.1515/9783110308426.

26. Da silva JJRF, Williams RJP (1991) The Biological Chemistry of the Elements: The Inorganic Chemistry of Life. Clarendon Press, Oxford.

27. Peters DG, Connor JR, Meadowcroft MD (2015) The relationship between iron dyshomeostasis and amyloidogenesis in Alzheimer's disease: Two sides of the same coin. Neurobiol Dis 81:49–65. https://doi.org/10.1016/j.nbd.2015.08.007.

28. Wang Z, Bussche AVD, Kabadi PK, Kane AB, Hurt RH (2013) Biological and Environmental Transformations of Copper-Based Nanomaterials. ACS Nano 7:8715–8727. https://doi.org/10.1021/nn403080y.

29. Bhati A, Anand SR, Saini D, Khare P, Dubey P, Sonkar SK (2018) Self-doped nontoxic red-emitting Mg–N-embedded carbon dots for imaging, Cu(ii) sensing and fluorescent ink. New J Chem 42:19548–19556. https://doi.org/10.1039/C8NJ04754E.

30. Anbu S, Paul A, Surendranath K, Sidali A, Pombeiro AJL (2021) Naphthalimide-phenanthroimidazole incorporated new fluorescent sensor for "turn-on" Cu^{2+} detection in living cancer cells. J Inorg Biochem 220:111466. https://doi.org/10.1016/j.jinorgbio.2021.111466.

31. Patir K, Gogoi K (2019) Nitrogen-doped carbon dots as fluorescence ON–OFF–ON sensor for parallel detection of copper(II) and mercury(II) ions in solutions as well as in filter paper-based microfluidic device. Nanoscale Adv 1:592–601. https://doi.org/10.1039/C8NA00080H.

32. Bhatt M, Bhatt S, Vyas G, Raval IH, Haldar S, Paul P (2020) Water-Dispersible Fluorescent Carbon Dots as Bioimaging Agents and Probes for Hg^{2+} and Cu^{2+} Ions. ACS Appl Nano Mater 3:7096–7104. https://doi.org/10.1021/acsanm.0c01426.

33. Yarur F, Macairan J, Naccache R (2019) Ratiometric detection of heavy metal ions using fluorescent carbon dots. Environ Sci Nano 6:1121–1130. https://doi.org/10.1039/C8EN01418C.

34. Sadak O, Sundramoorthy AK, Gunasekaran S (2017) Highly selective colorimetric and electrochemical sensing of iron (III) using Nile red functionalized graphene film. Biosens Bioelectron 89:430–436. https://doi.org/10.1016/j.bios.2016.04.073.

35. Ghaedi M, Shokrollahi A, Kianfar AH, Mirsadeghi AS, Pourfarokhi A, Soylak M (2008) The determination of some heavy metals in food samples by flame atomic absorption spectrometry after their separation-preconcentration on bis salicyl aldehyde, 1,3 propan diimine (BSPDI) loaded on activated carbon. J Hazard Mater 154:128–134. https://doi.org/10.1016/j.jhazmat.2007.10.003.

36. Xu Q, Liu X, Jiang Y, Wang P (2021) A Highly Sensitive and Selective Probe for the Colorimetric Detection of Mn(II) Based on the Antioxidative Selenium and Nitrogen Co-Doped Carbon Quantum Dots and $ABTS^{\bullet+}$. Front Chem 9:658105. https://doi.org/10.3389/fchem.2021.658105.

37. Liu P, Borrell PF, Bozic M, Kokol V, Oksman K, Mathew AP (2015) Nanocelluloses and their phosphorylated derivatives for selective adsorption of Ag^{+}, Cu^{2+} and Fe^{3+} from industrial effluents. J Hazard Mater 294:177–185. https://doi.org/10.1016/j.jhazmat.2015.04.001.

38. Wang W, Wu J, Xing Y, Wang Z (2022) Solvent-dependent red emissive carbon dots and their applications in sensing and solid-state luminescence. Sens Actuator B Chem 360:131645. https://doi.org/10.1016/j.snb.2022.131645.

39. Hashemi N, Mousazadeh MH (2021) Preparation of fluorescent nitrogen-doped carbon dots for highly selective on-off detection of Fe^{3+} ions in real samples. Opt Mater 121: 111515. https://doi.org/10.1016/j.optmat.2021.111515.

40. Zhu L, Shen D, Liu Q, Wu C, Gu S (2021) Sustainable synthesis of bright green fluorescent carbon quantum dots from lignin for highly sensitive detection of Fe^{3+} ions. Appl Surf Sci 565:150526. https://doi.org/10.1016/j.apsusc.2021.150526.

41. Atchudan R, Edison TNJI, Perumal S, Vinodh R, Sundramoorthy AK, Suresh Babu R, Lee YR (2021) Leftover Kiwi Fruit Peel-Derived Carbon Dots as a Highly Selective Fluorescent Sensor for Detection of Ferric Ion. Chemosensors 9:166. https://doi.org/10.3390/chemosensors9070166.

42. Das GS, Shim JP, Bhatnagar A, Tripathi KM, Kim TY (2019) Biomass-derived Carbon Quantum Dots for Visible-Light-Induced Photocatalysis and Label-Free Detection of Fe(III) and Ascorbic acid. Sci Rep 9:15084. https://doi.org/10.1038/s41598-019-49266-y.

43. Bhamore JR, Jha S, Park TJ, Kailasa SK (2018) Fluorescence sensing of Cu^{2+} ion and imaging of fungal cell by ultra-small fluorescent carbon dots derived from *Acacia concinna* seeds. Sens Actuator B Chem 277:47–54. https://doi.org/10.1016/j.snb.2018.08.149.

44. Sharma S, Tejwan N, Thakur S, Sharma V, Singh TA, Das J|, Das NC (2022) Synthesis of novel carbon dots from taurine for Cu^{2+} sensing and nanohybrid with ceria for visible light photocatalysis. Opt Mater 124:111995. https://doi.org/10.1016/j.optmat.2022.111995.

45. Rooj B, Dutta A, Islam S, Mandal U (2018) Green Synthesized Carbon Quantum Dots from Polianthes tuberose L. Petals for Copper (II) and Iron (II) Detection. J Fluoresc 28:1261–1267. https://doi.org/10.1007/s10895-018-2292-6.

46. Hao Y, Yu L, Li T, Chen L, Han X, Chai F (2023) The synthesis of carbon dots by folic acid and utilized as sustainable probe and paper sensor for Hg^{2+} sensing and cellular imaging. Spectrochim Acta A Mol Biomol Spectrosc 285:121865. https://doi.org/10.1016/j.saa.2022.121865.

47 Baskaya SK, Tahta B, Urus S, Eskalen H, Çeşme M, Özğan Ş (2022) Multifunctional B, N, P, and S-doped fluorescent carbon quantum dot synthesis from pigeon manure: highly effective Hg (II) sensor and fluorescent ink properties. Biomass Conv Bioref https://doi.org/10.1007/s13399-022-03017-8.

48 Zhang S, Jin L, Liu J, Wang Q, Jiao L (2020) A label-free yellow-emissive carbon dot-based nanosensor for sensitive and selective ratiometric detection of chromium (VI) in environmental water samples. Mater Chem Phys 248:122912. https://doi.org/10.1016/j.matchemphys.2020.122912.

49. Qing W, Chen K, Yang Y, Wang Y, Liu X (2020) Cu^{2+}-doped carbon dots as fluorescence probe for specific recognition of Cr(VI) and its antimicrobial activity. Microchem J 152:104262. https://doi.org/10.1016/j.microc.2019.104262.

50. Li X, Zhao L, Wu Y, Zhou A, Jiang X, Zhan Y, Sun Z (2022) Nitrogen and boron co-doped carbon dots as a novel fluorescent probe for fluorogenic sensing of Ce^{4+} and ratiometric detection of Al^{3+}. Spectrochim Acta A Mol Biomol Spectrosc 282:121638. https://doi.org/10.1016/j.saa.2022.121638.

51. Arumugham T, Alagumuthu M, Amimodu RG, Munusamy S, Iyer SK (2020) A sustainable synthesis of green carbon quantum dot (CQD) from *Catharanthus roseus* (white flowering plant) leaves and investigation of its dual fluorescence responsive behavior in multi-ion detection and biological applications. Sustainable Mater Tech 23:e00138. https://doi.org/10.1016/j.susmat.2019.e00138.

52. Raja S, Mattoso LHC (2020) Functionalized Polymer-Based Composite Photocatalysts, in: Naushad M, Rajendran S, Lichtfouse E (Eds) Green Photocatalysts Environmental Chemistry for a Sustainable World 34 Springer Cham pp 167–188. https://doi.org/10.1007/978-3-030-15608-4_7.

53. Shen H, Peppel T, Strunk J, Sun Z (2020) Photocatalytic Reduction of CO2 by Metal-Free-Based Materials: Recent Advances and Future Perspective. Sol RRL 4:1900546. https://doi.org/10.1002/solr.201900546.

54. Basavaraj N, Sekar A, Yadav R (2021) Review on green carbon dot-based materials for the photocatalytic degradation of dyes: fundamentals and future perspective. Mater Adv 2:7559–7582. https://doi.org/10.1039/D1MA00773D.

55. Vyas Y, Chundawat P, Dharmendra D, Punjabi PB, Ameta C (2021) Review on hydrogen production photocatalytically using carbon quantum dots: Future fuel. Int J Hydrog 46:37208–37241. https://doi.org/10.1016/j.ijhydene.2021.09.004.

56. Park YH, Murali G, Modigunta JKR, In I, In S (2020) Recent Advances in Quantum Dots for Photocatalytic CO_2 Reduction: A Mini-Review. Front Chem 9:734108. https://doi.org/10.3389/fchem.2021.734108.

57. Zhang Z, Yi G, Li P, Zhang X, Fan H, Zhang Y, Wang X, Zhang CA (2020) A minireview on doped carbon dots for photocatalytic and electrocatalytic applications. Nanoscale 12:13899–13906. https://doi.org/10.1039/D0NR03163A.

58. Wang Y, Liu X, Han X, Godin R, Chen J, Zhou W, Jiang C, Thompson JF, Mustafa KB, Shevlin SA, Durrant JR, Guo Z, Tang J (2020) Unique hole-accepting carbon-dots promoting selective carbon dioxide reduction nearly 100% to methanol by pure water. Nat Commun 11:2531. https://doi.org/10.1038/s41467-020-16227-3.

59. Li Q, Wang S, Sun Z, Wang H, Tang Q, Liu Y, Wang L, Wu Z (2019) Enhanced CH_4 selectivity in CO_2 photocatalytic reduction over carbon quantum dots decorated and oxygen doping g-C_3N_4. Nano Research 12:2749–2759. https://doi.org/10.1007/s12274-019-2509-2.

60. Colombo CA, Berton LHC, Diaz BG, Ferrari RA (2018) Macauba: a promising tropical palm for the production of vegetable oil. OCL 25:D108. https://doi.org/10.1051/ocl/2017038.

61. Corrêa AC, Carmona VB, Simão JA, Galvani F, Marconcini JM, Mattoso LHC (2019) Cellulose Nanocrystals from Fibers of Macauba (*Acrocomia Aculeata*) and Gravata (*Bromelia Balansae*) from Brazilian Pantanal. Polymers 11:1785. https://doi.org/10.3390/polym11111785.

62. Raja S, Buhl EM, Dreschers S, Schalla C, Zenke M, Sechi A, Mattoso LHC (2021) Curauá-derived carbon dots: Fluorescent probes for effective Fe(III) ion detection, cellular labeling and bioimaging. Mater Sci Eng C 129:112409. https://doi.org/10.1016/j.msec.2021.112409.

63. Hatchard CG, Parker CA (1956) A new sensitive chemical actinometer - II. Potassium ferrioxalate as a standard chemical actinometer. Proc R Soc Lond A 235:518–536. https://doi.org/10.1098/rspa.1956.0102.

64. Ding S, Gao Y, Ni B, Yang X (2021) Green synthesis of biomass-derived carbon quantum dots as fluorescent probe for Fe^{3+} detection. Inorg Chem Commun 130:108636. https://doi.org/10.1016/j.inoche.2021.108636.

65. Liang Y, Liu Y, Li S, Lu B, Liu C, Yang H, Ren X, Hou Y (2019) Hydrothermal growth of nitrogen-rich carbon dots as a precise multifunctional probe for both Fe^{3+} detection and cellular bio-imaging. Opt Mater 89:92–99. https://doi.org/10.1016/j.optmat.2019.01.008.

66. Atchudan R, Edison TNJI, Perumal S, Muthuchamy N, Lee YR (2020) Hydrophilic nitrogen-doped carbon dots from biowaste using dwarf banana peel for environmental and biological applications. Fuel 275: 117821. https://doi.org/10.1016/j.fuel.2020.117821.

67. Zulfajri M, Gedda G, Chang C, Chang Y, Huang GG (2019) Cranberry Beans Derived Carbon Dots as a Potential Fluorescence Sensor for Selective Detection of Fe^{3+} Ions in Aqueous Solution. ACS Omega 4:15382–15392. https://doi.org/10.1021/acsomega.9b01333.

68. Bhamore JR, Jha S, Park TJ, Kailasa SK (2018) Fluorescence sensing of Cu^{2+} ion and imaging of fungal cell by ultra-small fluorescent carbon dots derived from *Acacia concinna* seeds. Sens Actuator B Chem 277:47–54. https://doi.org/10.1016/j.snb.2018.08.149.

69. Gu D, Zhang P, Zhang L, Liu H, Pu Z, Shang S (2018) Nitrogen and phosphorus co-doped carbon dots derived from lily bulbs for copper ion sensing and cell imaging. Optical Materials 83:272–278. https://doi.org/10.1016/j.optmat.2018.06.012.

70. Emami E, Mousazadeh MH (2021) Green synthesis of carbon dots for ultrasensitive detection of Cu^{2+} and oxalate with turn on-off-on pattern in aqueous medium and its application in cellular imaging. J Photochem Photobiol 418:113443. https://doi.org/10.1016/j.jphotochem.2021.113443.

71. Radhakrishnan K, Panneerselvam P, Marieeswaran M (2019) A green synthetic route for the surface-passivation of carbon dots as an effective multifunctional fluorescent sensor for the recognition and detection of toxic metal ions from aqueous solution. Anal Methods 11: 490–506. https://doi.org/10.1039/C8AY02451K.

72. Salinas-Castillo A, Morales DP, Lapresta-Fernández A, Ariza-Avidad M, Castillo E, Martı´nez-Olmos A, Palma AJ, Capitan-Vallvey LF (2016) Evaluation of a reconfigurable portable instrument for copper determination based on luminescent carbon dots. Anal Bioanal Chem 408:3013–3020. https://doi.org/10.1007/s00216-016-9349-7.

73. Khose RV, Chakraborty G, Bondarde MP, Wadekar PH, Ray AK, Som (S) (2021) Red-fluorescent graphene quantum dots from guava leaf as a turn-off probe for sensing aqueous Hg(II). New J Chem 45:4617–4625. https://doi.org/10.1039/D0NJ06259F.

74. Pajewska-Szmyt M, Buszewski B, Gadzała-Kopciuch R (2020) Carbon dots as rapid assays for detection of mercury(II) ions based on turn-off mode and breast milk. Spectrochim Acta A Mol Biomol Spectrosc 236: 118320. https://doi.org/10.1016/j.saa.2020.118320.

75. Li L-S, Jiao X.-Y, Zhang Y, Cheng C, Huang K, Xu L (2018) Green synthesis of fluorescent carbon dots from Hongcaitai for selective detection of hypochlorite and mercuric ions and cell imaging. Sens Actuator B Chem 263:426–435. https://doi.org/10.1016/j.snb.2018.02.141.

76. Wang CY, Wang CF, Xu PP, Li AQ, Chen YJ, Zhuo KL (2016) Synthesis of cellulose-derived carbon dots using acidic ionic liquid as a catalyst and its application for detection of Hg^{2+}. J. Mater. Sci. 51: 861–867. https://doi.org/10.1007/s10853-015-9410-5.

77. He JL, Zhang HR, Zou JL, Liu YL, Zhuang JL, Xiao Y, Lei BF (2016) Carbon dots-based fluorescent probe for "off-on" sensing of Hg(II) and I^-. Biosens Bioelectron 79:531–535. https://doi.org/10.1016/j.bios.2015.12.084.

78. Xie Y, Cheng D, Liu X, Han A (2019) Green Hydrothermal Synthesis of N-doped Carbon Dots from Biomass Highland Barley for the Detection of Hg^{2+}. Sensors 19:3169. https://doi.org/10.3390/s19143169.

79. Gao X, Zhou X, Ma Y, Qian T, Wang C, Chu F (2019) Facile and cost-effective preparation of carbon quantum dots for Fe^{3+} ion and ascorbic acid detection in living cells based on the "on-off-on" fluorescence principle. Appl Surf Sci 469:911–916. https://doi.org/10.1016/j.apsusc.2018.11.095.

80. Luo X, Zhang W, Han Y, Chen X, Zhu L, Tang W, Wang J, Yue T, Li Z (2018) N, S co-doped carbon dots based fluorescent "on-off-on" sensor for determination of ascorbic acid in common fruits. Food Chem 258:214–221. https://doi.org/10.1016/j.foodchem.2018.03.032.

81. Chen K, Qing W, Hu W, Lu M, Wang Y, Liu X (2019) On-off-on fluorescent carbon dots from waste tea: Their properties, antioxidant and selective detection of CrO_4^{2-}, Fe^{3+}, ascorbic acid and L-cysteine in real samples. Spectrochim Acta A Mol Biomol Spectrosc 213:228–234. https://doi.org/10.1016/j.saa.2019.01.066.

82. Fernando KAS, Sahu S, Liu Y, Lewis WK, Guliants EA, Jafariyan A, Wang P, Bunker CE, Sun Y (2015) Carbon Quantum Dots and Applications in Photocatalytic Energy Conversion. ACS Appl Mater Interfaces 7:8363−8376. https://doi.org/10.1021/acsami.5b00448.

83. Silva GTST, Nogueira AE, Oliveira JA, Torres JA, Lopes OF, Ribeiro C (2019) Acidic surface niobium pentoxide is catalytic active for CO_2 photoreduction. Appl Catal B Environ 242: 349–357. https://doi.org/10.1016/j.apcatb.2018.10.017.

84. Han M, Zhu S, Lu S, Song Y, Feng T, Tao S, Liu J, Yang B (2018). Recent progress on the photocatalysis of carbon dots: Classification, mechanism and applications. Nano Today 19: 201–218. https://doi.org/10.1016/j.nantod.2018.02.008.

85. Ulmer U, Dingle T, Duchesne PN, Morris RH, Tavasoli A, Wood T, Ozin G (2019) Fundamentals and applications of photocatalytic CO_2 methanation. Nat Commun 10:3169. https://doi.org/10.1038/s41467-019-10996-2.

86. Liu Z, Wang Z, Qing S, Xue N, Jia S, Zhang L, Li L, Li N, Shi L, Chen J (2018) Improving Methane Selectivity of Photo-Induced CO_2 Reduction on Carbon Dots through Modification of Nitrogen-Containing Groups and Graphitization. Appl Catal B, Environ 232: 86-92. https://doi.org/10.1016/j.apcatb.2018.03.045.

Graphical Abstract